

# Research on testing the characteristics of hydrogel film by using a long-period fiber grating

Xiujuan Yu,<sup>1,2,\*</sup> Min Zhang,<sup>1</sup> Paul Childs,<sup>1</sup> Liwei Wang,<sup>1</sup> Ming Lei,<sup>1</sup>  
Yanbiao Liao,<sup>1</sup> Jian Ju,<sup>3</sup> and Win Jin<sup>3</sup>

<sup>1</sup>Department of Electronic Engineering, Tsinghua University, Beijing, 100080, China

<sup>2</sup>Optical Fiber Research Institute of Heilongjiang University, Haerbin, 150080, China

<sup>3</sup>Department of Electrical Engineering, The Hong Kong Polytechnic University, Hung Hom, Kowloon, Hong Kong

\*Corresponding author: yuxj06@mails.tsinghua.edu.cn

Received 7 January 2009; revised 26 February 2009; accepted 23 March 2009;  
posted 26 March 2009 (Doc. ID 106024); published 7 April 2009

A method for testing the physical and optical properties of hydrogel thin films is reported based on using long-period fiber gratings. For humidity levels from 50% to 70% RH, a wavelength decrease of 11.0 nm is observed, with a sensitivity of 0.6 nm/%RH. For humidity levels from 70% to 98% RH, a wavelength increase of 6.3 nm is seen, with a sensitivity of 0.2 nm/%RH. For humidity levels greater than 60% RH, the transmission loss at resonance increases rapidly, showing a high degree of sensitivity of 0.5 dB/%RH. The blueshift of the wavelength was seen to be due to a thickening of the overlay, while the redshift of wavelength is due to the contribution of the drop in refractive index of the overlay. The results match well with what is expected theoretically. © 2009 Optical Society of America

OCIS codes: 310.6860, 310.7060, 060.2300, 060.2310, 060.2370.

## 1. Introduction

Hydrogels are three-dimensional (3D), cross-linked hydrophilic polymer networks that can absorb water and swell. Intelligent hydrogels respond to various stimuli such as temperature [1], pH [2], electric field [3], stress [4], and light [5] through volume or conformation changes, and they can be widely used in many fields, such as bioseparations [6], drug delivery [7,8], sensors [9], and intelligent surfaces [10]. When the hydrogels absorb water, their physical and optical properties will change. While a variety of techniques can be used to study the changes exhibited by the bulk hydrogel, the number of analytical methods used to study thin films of hydrogel is limited.

A long-period fiber grating (LPFG) is a photoinduced periodic modulation of the refractive index of the core of a single-mode optical fiber. Its period is generally in the range of 100  $\mu\text{m}$  to 1 mm. The

LPFG couples light between the guided core mode and different copropagating cladding modes in a single-mode fiber. Because the cladding modes suffer from high attenuation, a series of attenuation bands in the fiber transmission spectrum can be seen, each centered at a resonant wavelength that depends on the effective index of the coupled modes and the grating pitch. The resonant wavelength and amplitude of the attenuation bands of an LPFG are very sensitive to perturbations of the external surroundings, and thus LPFGs can be used to measure temperature [11], strain [12], refractive index [13], solution concentration [14], and pH [15]. In recent years a lot of research has focused on high-refractive-index coated LPFGs to enhance the sensor's sensitivity to ambient refractive index changes. Rees *et al.* [16] proposed a LPFG with Langmuir–Blodgett thin-film overlays and demonstrated that the central wavelength of the attenuation bands of an LPFG depends on the optical thickness of the overlay material and that the sensitivity of this effect occurs most readily at a certain overlay thickness. Del Villar

*et al.* [17,18] reported a numerical and experimental investigation of cladding mode reorganization in high-refractive-index coated LPFGs and demonstrated that high-refractive-index overlay deposition can cause the cladding modes to become overlay-guided modes at a certain overlay thickness, thus creating a strong redistribution of the cladding modes and leading to rapid shifts of the resonance wavelength of the attenuations bands.

In this paper, we developed a novel method to test the physical and optical characteristics of hydrogel films by using an LPFG. A nanoscale thin layer of hydrogel film is deposited on the cladding of a LPFG. The thickness of the overlay is chosen to maximize the sensitivity of the LPFG. When the ambient humidity is increased, the hydrogel absorbs water from the air, and its characteristics (volume and refractive index) will change, each leading to a change in the effective index of the cladding modes. Because of the multiparameter sensing capability of LPFGs [19], these two effects can both be measured (in this case utilizing changes to the resonant wavelength shift and amplitude of an attenuation band) and separated out (whereas in using conventional single-parameter sensing, this is impossible). The proposed method possesses the advantages of having a high sensitivity, being low cost, and being able to offer on-line, real-time measurements of the film characteristics while the hydrogel is absorbing or releasing the water.

## 2. Theory

In a standard LPFG, the phase matching condition between the core mode and the  $\nu$ th copropagating cladding mode is achieved at a resonant wavelength  $\lambda_\nu$  when

$$\lambda_\nu = [n_{\text{eff,co}}(\lambda_\nu) - n_{\text{eff,cl}}^\nu(\lambda_\nu)]\Lambda, \quad (1)$$

where  $\Lambda$  is the grating period,  $n_{\text{eff,co}}(\lambda_\nu)$  is the effective index of the fundamental core mode, and  $n_{\text{eff,cl}}^\nu(\lambda_\nu)$  is the effective index of the  $\nu$ th cladding mode. The effective indices of the cladding modes are strongly dependent on the refractive index of the surrounding environment, and thus the resonant wavelength is sensitive to the change of the refractive index of the surrounding environment.

The depth of the attenuation band is influenced mainly by two factors: the length of the grating and the cross coupling coefficient between the core mode and the cladding mode that couple at the resonance wavelength, which can be expressed approximately as

$$T_\nu = 1 - \sin^2(\kappa_\nu L), \quad (2)$$

where  $L$  is the length of the LPFG and  $\kappa_\nu$  is the coupling coefficient of the  $\nu$ th cladding mode, which depends on the overlap integral of the core and cladding mode and the photoinduced refractive index modulation.

The mode eigenvalue equation can be determined by applying the four-layer step-index waveguide boundary conditions to Maxwell's equations (Fig. 1 shows the four-layer structure of the LPFG). The electromagnetic fields of a guided mode in a four-layered structure can be described by using a cylindrical coordinate system,  $(r, \phi, z)^T$ , and take the following form for each independent layer [20]:

$$\mathbf{E}_j = \begin{pmatrix} \frac{\partial \Psi}{r \partial \phi} - \frac{\beta}{\omega \epsilon_j} \frac{\partial \Phi}{\partial r} \\ -\frac{\partial \Psi}{\partial r} - \frac{\beta}{\omega \epsilon_j} \frac{\partial^2 \Phi}{\partial r \partial \phi} \\ -\frac{k^2 n_j^2 - \beta^2}{i \omega \epsilon_j} \Phi \end{pmatrix}, \quad \mathbf{H}_j = \begin{pmatrix} \frac{\partial \Phi}{r \partial \phi} + \frac{\beta}{\omega \mu} \frac{\partial \Psi}{\partial r} \\ -\frac{\partial \Phi}{\partial r} + \frac{\beta}{\omega \mu} \frac{\partial^2 \Psi}{\partial r \partial \phi} \\ \frac{k^2 n_j^2 - \beta^2}{i \omega \mu} \Psi \end{pmatrix}. \quad (3)$$

Here the subscript  $j$  ( $j = 1, 2, 3, 4$ ) indicates the layer number,  $\beta$  is the propagation constant of a particular mode,  $\omega$  stands for the light circular frequency,  $\epsilon_j$  and  $\mu$  denote, respectively, the electric permittivity and magnetic permeability for each  $j$ th layer in the four-layer structure, and  $\Psi$  and  $\Phi$  are the scalar Debye potentials satisfying the usual wave equations such that

$$\left( \frac{\partial^2}{\partial r^2} + \frac{\partial}{r \partial r} + \frac{\partial^2}{r^2 \partial \phi^2} + k^2 n_j^2 - \beta^2 \right) (\Phi, \Psi) = 0. \quad (4)$$

The Debye potentials  $\Psi$  and  $\Phi$  can be expressed as follows:

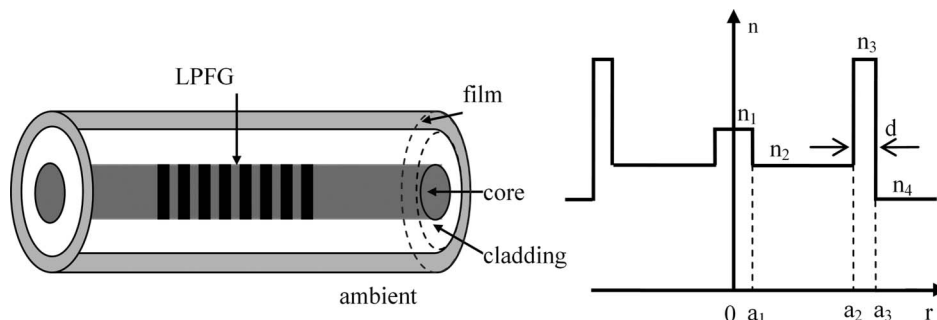


Fig. 1. Schematic diagram of the four-layer waveguide structure.

$$\Phi(r) = \begin{cases} A_1 Z_{\nu,1}(u_1 r) \\ A_2 Z_{\nu,2}(u_2 r) + B_2 T_{\nu,2}(u_2 r) \\ A_3 Z_{\nu,3}(u_3 r) + B_3 T_{\nu,3}(u_3 r) \\ B_4 K_{\nu}(w_4 r) \end{cases},$$

$$\Psi(r) = \begin{cases} C_1 Z_{\nu,1}(u_1 r) & r \leq a_1 \\ C_2 Z_{\nu,2}(u_2 r) + D_2 T_{\nu,2}(u_2 r) & a_1 < r \leq a_2 \\ C_3 Z_{\nu,3}(u_3 r) + D_3 T_{\nu,3}(u_3 r) & a_2 < r \leq a_3 \\ D_4 K_{\nu}(w_4 r) & r > a_3 \end{cases}, \quad (5)$$

where

$$Z_{\nu,j}(x) = \begin{cases} J_{\nu}(x) \\ I_{\nu}(x) \end{cases}, \quad T_{\nu,j}(x) = \begin{cases} Y_{\nu}(x) & n_{\text{eff}} < n_j \\ K_{\nu}(x) & n_{\text{eff}} > n_j \end{cases},$$

$$u_j = \frac{2\pi}{\lambda} \sqrt{|n_j^2 - n_{\text{eff}}^2|}, \quad w_4 = \frac{2\pi}{\lambda} \sqrt{n_{\text{eff}}^2 - n_4^2}, \quad (6)$$

and  $J_{\nu}$  and  $I_{\nu}$  are the ordinary Bessel functions of the first and second kind, respectively, of order  $\nu$ .  $Y_{\nu}$  and  $K_{\nu}$  are the modified Bessel functions of first and second kind, respectively, of order  $\nu$ .  $a_1$  and  $a_2$  are the core and cladding radii, and  $a_3 - a_2$  is the thickness of the hydrogel film.  $n_1, n_2, n_3$  and  $n_4$  are the core, cladding, hydrogel film, and ambient indices, respectively.  $n_{\text{eff}}$  is the effective index, which can be obtained by finding the numerical solution of the eigenvalue equation by the continuity condition of the transverse fields.

The refractive index of a two-phase structure can be approximately expressed by the equation

$$n_{2p} = \sqrt{(1-V)n_0^2 + Vn_p^2}, \quad (7)$$

where  $n_{2p}$  is the effective refractive index of the structure,  $n_0$  and  $n_p$  are the refractive indices of the structure and the pores, respectively, and  $V$  is the volume fraction of the pores. The dry, collapsed hydrogel has a refractive index of about  $n_0 = 1.55$ , while water has a value of  $n_p = 1.33$ . As the hydrogel absorbs more water, the average index will monotonically decrease.

The calculation results are shown in Figs. 2 and 3 for the parameters  $a_1 = 4.15 \mu\text{m}$ ,  $a_2 = 62.5 \mu\text{m}$ ,  $n_1 = 1.458$ ,  $n_2 = 1.45$ ,  $n_4 = 1$ . In the calculation, we use the ninth cladding mode because the resonant wavelength of the uncoated LPFG for this mode is about 1550 nm and is thus readily measured by using a C band source. In this experiment, the coated LPFG is exposed to the air, where the humidity is changed. Thus the ambient refractive index can be fixed to 1. When the humidity changes, the hydrogel absorbs water from the ambient environment and will swell in volume, leading to an increase in the overlay thickness and a decrease in the refractive index. Figure 2 shows that the resonant wavelength of the coated LPFG shifts to a longer wavelength when the overlay's refractive index increases (when the

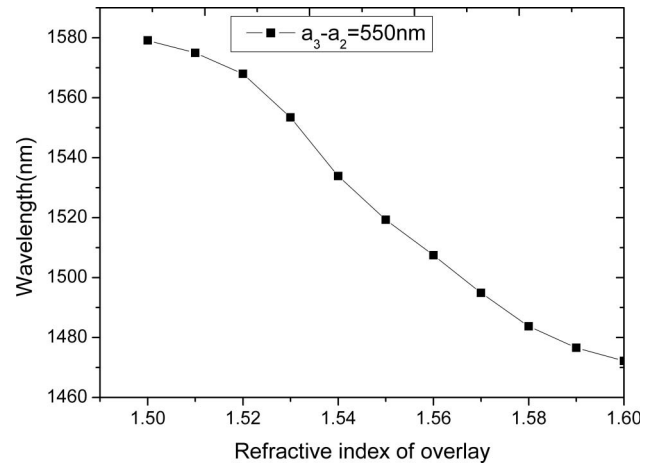


Fig. 2. Wavelength shift versus refractive index of overlay.

optimal overlay thickness is chosen to be 550 nm). Figure 3 shows that the resonant wavelength suffers a blueshift (a shift to shorter wavelengths) with an increase of the overlay's thickness (the overlay's index is set as 1.55 in the graph).

### 3. Experimental Results and Discussion

The LPFG used in the experiment was fabricated by high-frequency  $\text{CO}_2$  laser pulses in a conventional single-mode fiber with a period of  $400 \mu\text{m}$  and a period number of 40. A thin film of hydrogel was deposited on the LPFG by the dip coating technique. Dip coating is a simple and effective method that can control the overlay thickness by varying the solution density and extraction velocity.

To carry out the tests of the hydrogel, the coated LPFG was fixed on a V groove and placed in a programmable temperature and humidity chamber (TYH-1P Gaoyu Technical Co., Ltd.) where both temperature and humidity can be controlled exactly. Figure 4 shows the schematic diagram of the experimental setup. One end of the LPFG was connected to an amplified spontaneous emission (ASE) broadband light source, while the other end was connected to an

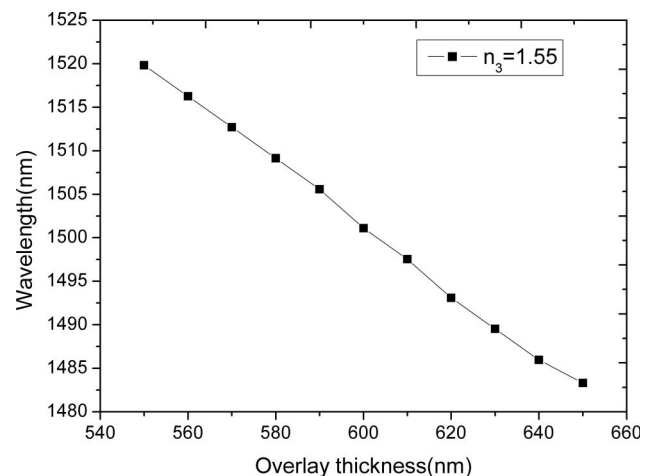


Fig. 3. Wavelength shift versus the thickness of overlay.

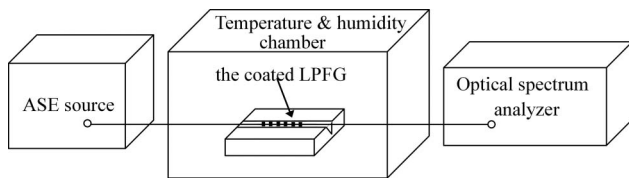


Fig. 4. Schematic diagram of the experimental setup.

optical spectrum analyzer (86140B Agilent) with a wavelength resolution of 0.1 nm and a level resolution of 0.01 dB. The transmission spectrum of the LPFG is shown in Fig. 5, where the solid and dashed curves represent the uncoated and the coated LPFG, respectively. The depth of the resonant dip of the coated LPFG was significantly reduced compared with the uncoated LPFG. Meanwhile, the resonant wavelength shifted to the shorter wavelength side.

The physical and optical properties of the hydrogel film were tested by using the coated LPFG. Specifically, the humidity sensitivities due to changes in both the thickness and refractive index of the films were measured under a variety of environmental conditions. We increased the relative humidity (RH) range from 25% to 98% (the humidity range of the chamber) to test the hydrogel behavior during the process of absorbing water. The temperature of the chamber was held constant at 25°C during the test with fluctuations of less than 0.5°C. The temperature accuracy was  $\pm 0.3^\circ\text{C}$ , and the humidity resolution was 0.1% RH. The transmission spectrum's response to the humidity is shown in Fig. 6. The data have been normalized with respect to the optical source spectrum to outline the differences. The value of the resonant dip and wavelength are plotted in Fig. 7 for different values of RH ranging from 25% to 98%. In the double-y plot shown in Fig. 7, the left- and right-hand y axes denote the resonant wavelength and the minimum transmission value, respectively. For humidity levels less than 40% RH, the wavelength and the resonant dip were barely affected by the humidity and were kept to a

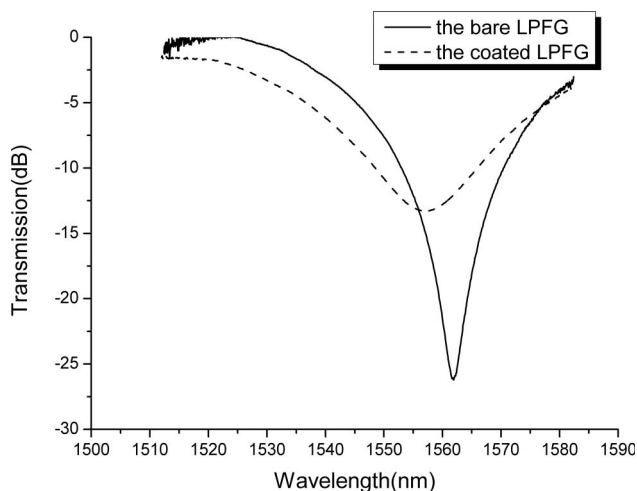


Fig. 5. Transmission spectrum of the LPFG.

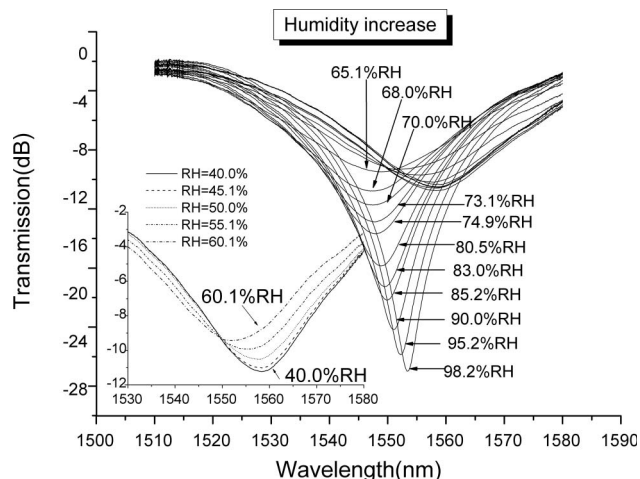


Fig. 6. Changes in the transmission spectrum of the LPFG with an increase in humidity.

stable level. This behavior may be dominated by the intrinsic material properties of the hydrogel film, since there was little or no water absorbed by the material when the humidity was less than 40% RH. When the RH was greater than 40%, an interesting phenomenon appeared. The resonant wavelength exhibited a significant blueshift with an almost linear change of 11.0 nm over the humidity levels between 50% and 70% RH, giving a sensitivity of 0.6 nm/%RH. For values of RH greater than 70%, the resonant wavelength shifted to a longer wavelength, and the LPFG suffered a redshift of 6.3 nm up to 98% RH with a sensitivity of 0.2 nm/%RH.

As the humidity is increased, the depth of transmission spectrum also changed but with an opposite trend compared with the resonant wavelength. Over the humidity range of 25% to 60% RH, the amplitude of the attenuation band changed only slightly, decreasing by about 2.5 dB; this phenomenon is shown in the lower left-hand graph of Fig. 6. When the humidity was greater than 65%, the resonant dip depth suffered a significant and almost linear increase with a span of 16.9 dB up to 98% RH and a sensitivity of

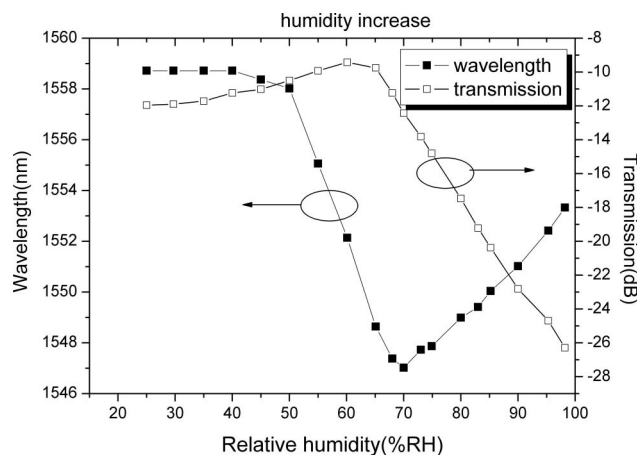


Fig. 7. Resonant dip depth and wavelength versus percent RH with increasing percent RH values.

0.5 dB/%RH. When the humidity was 98% RH, the resonant dip depth of the coated LPFG recovered the original level of the uncoated LPFG. The reason for this experimental phenomenon will be discussed in detail below.

To test the behavior of the coated LPFG as water is being desorbed from the hydrogel, a test for decreasing levels of humidity was also performed. When the humidity was decreased from 98% to 25% RH, the resonant dip and wavelength underwent an opposite change trend compared with the case of increasing humidity. At humidity levels greater than 40% RH, the values of the resonant wavelength and dip depth during the increase and decrease of humidity agreed with each other well at the same point, which can be seen in Fig. 8. However, the two curves in both Figs. 8 and 9 are offset from each other. This phenomenon may be caused by some water left in the hydrogel. It is harder for the hydrogel to release water than to absorb it, and it also takes longer to release it. If more time is provided to let the hydrogel recover its original structure, the phenomenon may be decreased. The above experimental results were repeated several times and were found to be reproducible.

In this experiment, the humidity-sensitive hydrogel operates via changes in its physical and optical properties. When the ambient humidity is increased, the hydrogel absorbs water from the air to reach a new equilibrium. As the structure absorbs the water, it deforms from its previous equilibrium, contracted structure, attempting to swell in volume. The swelling causes a thickness increase of the hydrogel overlay film. The shift to shorter resonant wavelengths is the result of swelling. As the humidity changes from 25% to 40% RH, the resonant wavelength of the LPFG remains stable. This stability is produced by the intrinsic material properties of the hydrogel, since there is little or no water absorbed by the material when the humidity is low. When the humidity is increased from 40% to 70% RH, the LPFG first suffers a wavelength blueshift. From the theoretical analysis in Section 2, we know that when the thickness of the overlay is increased, the resonant wave-

It should be remembered that as the hydrogel structure is absorbing water from the air, the water brought into the hydrogel structure will change the structure's refractive index, bringing the average of the water-hydrogel composite down with more water added. The refractive index of a two-phase structure can be expressed by Eq. (7). As the hydrogel absorbs more water, the average index will monotonically decrease. This effect is dominant when the RH is greater than 70%, bringing a redshift to the resonant wavelength. The analysis in Section 2 shows that the resonant wavelength is shifted to a longer wavelength when the refractive index of the coated film is decreased. Meanwhile, the drop in the refractive index of the overlay is opposed to the effect of the wavelength shift due to the structure swelling; the former causes the wavelength to shift to a shorter value, while the latter results in the wavelength's shifting to a longer wavelength. Thus we can conclude that as the RH changes from 70% to 98%, the shift to longer wavelengths is due purely to the reduction of the refractive index. There is a similar change for the resonant dip depth, but with the opposite trend. With an increase of the humidity, the resonant dip depth has a slight initial reduction and then suffers a rapid increase. This means that the thickness increase and refractive index decrease of the deposition overlay have different relative effects on the coupling strength and resonant wavelength, with the two strongest effects being those relating the swelling of the coating to the resonant wavelength and changes in the refractive index to the coupling strength. These phenomena need further theoretical and experimental investigation, and the work is ongoing.

As the curves of Fig. 7 often have two different values of percent RH for a given resonant wavelength or transmission dip depth, it is impossible to determine which is the true percent RH value based on one of these parameters alone. However, when both parameters are known, the correct value of the percent RH can be determined. An approximate piecewise linear fit to the curves of Fig. 7 gives the inversion algorithm for determining the humidity for this particular sensor as

---


$$\%RH = \begin{cases} 100\% - 2.01\%/dB(T + 27.4 \text{ dB}) & T < -12 \text{ dB} \\ 50\% - 1.66\%/nm(\lambda_v - 1558.1 \text{ nm}) & T > -12 \text{ dB}, \lambda_v < 1558 \text{ nm}, \\ \text{indeterminate} (< 50\%) & \lambda_v > 1558 \text{ nm} \end{cases} \quad (8)$$


---

length is shifted to a shorter wavelength. The experimental results agree with those of the theoretical analysis. So the blueshift of wavelength for ranges from 40% to 70% RH is due to the hydrogel structure's swelling.

where  $T$  is the resonant dip depth in decibels. The way in which both parameters can be used to determine the humidity is another case that shows how the multiparameter sensing capability of LPFGs is essential.

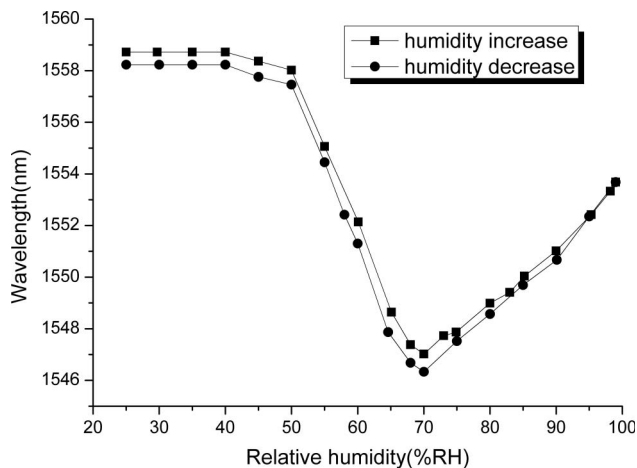


Fig. 8. Resonant wavelength versus percent RH for a full humidity cycle (increase then decrease).

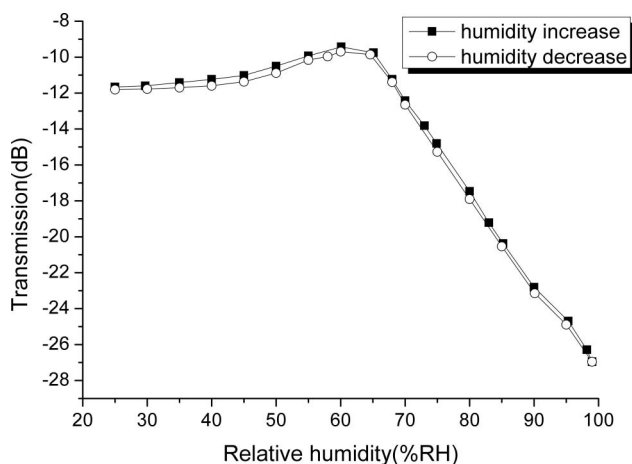


Fig. 9. Resonant dip depth versus percent RH for a full humidity cycle (increase then decrease).

#### 4. Conclusions

We developed and experimentally investigated a novel method for testing the physical and optical properties of hydrogel thin films by using coated LPFGs. The hydrogel coated LPFG was exposed to varying levels of humidity. When the humidity was increased, the change in the characteristics of the LPFG in both the transmission loss and wavelength at resonance reflected the changes to the physical and optical properties of the hydrogel. For humidity levels from 50% to 70% RH, the wavelength decreased by 11.0 nm, with a sensitivity of 0.6 nm/%RH. For humidity levels from 70% to 98% RH, the wavelength increased by 6.3 nm, with a sensitivity of 0.2 nm/%RH. For humidity levels greater than 60% RH, the transmission loss at resonance increased rapidly, showing a high degree of sensitivity of 0.5 dB/%RH. The blueshift of the wavelength was seen to be due to a thickening of the overlay, while the redshift of the wavelength was due to the contribution of the drop in the refractive index of the overlay. The coated LPFG was highly sensitive and could

perform measurements of the hydrogel thin film while absorbing water or desorbing water in real time. The experimental results also showed that the LPFG coated with hydrogel possessed good repeatability and could work efficiently for continuous testing.

This work was supported by NSFC of China through grant 60629401. The authors thank Prof. X.-G. Wang and Dr. J. Zhang of the Department of Chemistry Engineering, Tsinghua University, for composing the hydrogels.

#### References

1. T. Tanaka, D. Fillmore, S.-T. Sun, I. Nishio, G. Swislow, and A. Shah, "Phase transition in ionic gels," *Phys. Rev. Lett.* **45**, 1636–1639 (1980).
2. G. M. Eichenbaum, P. F. Kiser, S. A. Simon, and D. Needham, "pH and ion-triggered volume response of anionic hydrogel microspheres," *Macromolecules* **31**, 5084–5093 (1998).
3. T. Shiga, "Deformation and viscoelastic behavior of polymer gels in electric fields," *Adv. Polym. Sci.* **134**, 131–163 (1997).
4. A. Suzuki and T. Ishii, "Phase coexistence of neutral polymer gels under mechanical constraint," *J. Chem. Phys.* **110**, 2289–2296 (1999).
5. S. Juodkazis, N. Mukai, R. Wakaki, A. Yamaguchi, S. Matsuo, and H. Misawa, "Reversible phase transitions in polymer gels induced by radiation forces," *Nature* **408**, 178–181 (2000).
6. I. Y. Galaev, M. N. Gupta, and B. Mattiasson, "Use smart polymers for bioseparations," *Chemtech* **26**, 19–25 (1996).
7. A. S. Hoffman, "Intelligent polymers (in medicine and biotechnology)," in *Encyclopedia of Polymeric Materials* (CRC Press, 1996), pp. 3282–3292.
8. I. Y. Galaev and B. Mattiasson, "'Smart' polymers and what they could do in biotechnology and medicine," *Trends Biotechnol.* **17**, 335–340 (1999).
9. A. S. Hoffman, P. S. Stayton, V. Bulmus, G. Chen, J. Chen, C. Cheung, A. Chilkoti, Z. Ding, L. Dong, R. Fong, C. A. Lackey, C. J. Long, M. Miura, J. E. Morris, N. Murthy, Y. Nabeshima, T. G. Park, O. W. Press, T. Shimoboji, S. Shoemaker, H. J. Yang, N. Monji, R. C. Nowinski, C. A. Cole, J. H. Priest, J. M. Harris, K. Nakamae, T. Nishino, and T. Miyata, "Really smart bioconjugates of smart polymers and receptor proteins," *J. Biomed. Mater. Res.* **52**, 577–586 (2000).
10. N. Nath and A. Chilkoti, "Creating 'smart' surfaces using stimuli responsive polymers," *Adv. Mater.* **14**, 1243–1247 (2002).
11. V. Bhatia and A. M. Vengsarkar, "Optical fiber long-period grating sensors," *Opt. Lett.* **21**, 692–694 (1996).
12. M. Yokota, H. Oka, and T. Yoshino, "Mechanically induced long period fiber grating and its application for distributed sensing," in *15th Optical Fiber Sensors Conference Technical Digest, 2002. OFS 2002* (IEEE, 2002), pp. 135–138.
13. H. J. Patrick, A. D. Kersey, and F. Bucholtz, "Analysis of the response of long period fiber gratings to external index of refraction," *J. Lightwave Technol.* **16**, 1606–1612 (1998).
14. R. Falciai, A. G. Mignani, and A. Vannini, "Long period gratings as solution concentration sensors," *Sens. Actuators B* **74**, 74–77 (2001).
15. J. L. Elster, "Long period grating-based pH sensors for corrosion monitoring," M.S. thesis (Virginia Polytechnic Institute and State University, 1999).
16. N. D. Rees, S. W. James, R. P. Tatam, and G. J. Ashwell, "Optical fiber long-period gratings with Langmuir–Blodgett thin-film overlays," *Opt. Lett.* **27**, 686–688 (2002).

17. I. Del Villar, M. Achaerandio, I. R. Matias, and F. J. Arregui, "Deposition of overlays by electrostatic self-assembly in long-period fiber gratings," *Opt. Lett.* **30**, 720–722 (2005).
18. I. Del Villar, I. R. Matias, F. J. Arregui, and P. Lalanne, "Optimization of sensitivity in long period fiber gratings with overlay deposition," *Opt. Express* **13**, 56–69 (2005).
19. V. Bhatia, D. Campbell, and R. O. Claus, "Simultaneous strain and temperature measurement with long-period gratings," *Opt. Lett.* **22**, 648–650 (1997).
20. C. Tsao, *Optical Fibre Waveguide Analysis* (Oxford U. Press, 1992).